Dalton Transactions

PAPER

View Article Online
View Journal | View Issue

Open Access Article. Published on 19 July 2016. Downloaded on 12/4/2025 9:06:27 PM.
This article is licensed under a Creative Commons Attribution-NonCommercial 3.0 Unported Licence.

Cite this: *Dalton Trans.*, 2016, **45**, 12854

Functionalized phosphonates as building units for multi-dimensional homo- and heterometallic 3d–4f inorganic–organic hybrid-materials†

C. Köhler and E. Rentschler*

Received 20th May 2016,
Accepted 18th July 2016

DOI: 10.1039/c6dt02023b

www.rsc.org/dalton

Using the multifunctional ligand **H$_4$L** (2,2′-bipyridinyl-5,5′-diphosphonic acid), a new family of inorganic–organic hybrid-materials was prepared. The ligand shows a very high flexibility regarding the coordination mode, leading to a large structural diversity. The compounds **1a**, **1b** ([M(**H$_2$L**)(H$_2$O)$_4$]·2.5H$_2$O; M = Co^{2+} (**a**), Ni^{2+} (**b**)), **2** ([Gd$_2$(**H$_2$H′L**)$_2$(**H$_2$H′$_2$L**)(H$_2$O)$_6$]Cl$_4$·14H$_2$O), **3a**, **3b**, **3c** ([MCo(III)(**H$_2$L**)$_3$(H$_2$O)$_2$]·6.5H$_2$O; M = Gd^{3+} (**a**), Dy^{3+} (**b**) and Tb^{3+} (**c**)), and **4** ([GdNi(II)(**H$_2$L**)$_3$(H$_2$O)$_3$]NaCl·6H$_2$O) were isolated and characterized with single crystal X-ray diffraction. Depending on the used metal ions and on the stoichiometry, either discrete entities (0D), extended 2D layers or 3D frameworks were obtained. In contrast to the general approach in phosphonate chemistry, the compounds were prepared without hydrothermal synthesis, but under ambient pressure. Variable temperature magnetic measurements were carried out to determine the magnetic properties.

Introduction

The field of inorganic–organic hybrid-materials[1,2] shows an enormous potential in a broad spectrum of applications, such as adsorption/desorption, catalysis, functionalization of surfaces, nanomaterials or photoluminescent devices.[3–12] Additionally, the incorporation of open-shell transition metal ions or rare earth elements into these hybrids yielded a large number of magnetic materials, which exhibit several highly relevant properties from the field of molecular magnetism, *e.g.* long range magnetic ordering, single chain magnetism, large magnetocaloric effect or slow relaxation of magnetisation.[13–21]

Whereas the predominant type of inorganic–organic hybrid-materials is of homometallic nature,[22,23] the first heterometallic systems by Gatteschi *et al.* date back to 1985.[24] However, they are not as extensively studied as homometallic compounds, mostly due to their much smaller number.[25] A reason for the lack of heterometallic complexes is the much larger effort their synthesis bear. The challenge in the design of heterometallic compounds originates in the competition of different metal ions for the same or similar coordination sites.[26] One approach to overcome this problem is to make use of the desire of different sorts of metal ions for different coordination environments.[27,28]

We followed this strategy by employing a bipyridine based ligand, which contains additionally two phosphonate functionalities. While the bipyridine site shows a well-documented readiness for the coordination of transition metal ions,[29] the phosphonate groups offer perfect coordination condition for lanthanide ions due to the strong oxophilicity of the rare earth elements.[30–33] And although the phosphonate group is known for its highly divers modes of coordination, it's coordination can be fine-tuned by altering its charge by changing the pH value, making it very valuable for the task.[34]

We therefore employed the ligand 2,2′-bipyridinyl-5,5′-diphosphonic acid (**H$_4$L** or **H$_3$H′L**, see Scheme 1), first synthesized in 1998 by Penicaud *et al.*[35] It contains both functionalities mentioned above, which show a certain distinction in their coordination capabilities. To the best of our knowledge,

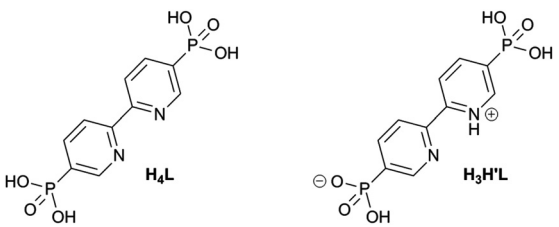

Scheme 1 Ligand **H$_4$L** or **H$_3$H′L**.

Institute of Inorganic and Analytical Chemistry, Johannes Gutenberg University Mainz, Duesbergweg 10-14, 55128 Mainz, Germany.
E-mail: rentschler@uni-mainz.de; http://www.ak-rentschler.chemie.uni-mainz.de

† Electronic supplementary information (ESI) available. CCDC 1477300–1477307. For ESI and crystallographic data in CIF or other electronic format see DOI: 10.1039/c6dt02023b

This journal is © The Royal Society of Chemistry 2016

Open Access Article. Published on 19 July 2016. Downloaded on 12/4/2025 9:06:27 PM.
This article is licensed under a Creative Commons Attribution-NonCommercial 3.0 Unported Licence.

Table 1 Crystallographic data for compounds **2**–**4**. Measurements were conducted at 173 K

	2	**3a**	**3b**	**3c**	**4**
Empirical formula	$C_{30}H_{42}Cl_4Gd_2N_6O_{38}P_6$	$C_{30}H_{27.5}CoGdN_6O_{26.5}P_6$	$C_{30}H_{25}CoDyN_6O_{26.5}P_6$	$C_{30}H_{27}CoN_6O_{26}P_6Tb$	$C_{30}H_{22}ClGdN_6NaNiO_{27}P_6$
Formula weight	1736.81	1298.08	1300.81	1291.24	1358.75
Crystal system	Triclinic	Monoclinic	Monoclinic	Monoclinic	Monoclinic
Space group	$P\bar{1}$	$C2/c$	$C2/c$	$C2/c$	$C2$
a/Å	10.362(3)	25.1648(18)	25.1186(12)	25.203(2)	22.6611(11)
b/Å	10.819(3)	17.1628(12)	17.0759(9)	17.0993(14)	16.9747(8)
c/Å	14.686(4)	23.0284(18)	22.9551(14)	22.983(2)	15.2845(7)
α/°	104.138(7)	90	90	90	90
β/°	100.605(7)	116.436(2)	116.0600(10)	116.064(2)	106.794(2)
γ/°	98.755(7)	90	90	90	90
V/Å^3	1535.5(7)	8905.9(11)	8845.0(8)	8897.4(13)	5628.7(5)
Z	1	8	8	8	4
ρ_{calc}/g cm^{-3}	1.878	1.936	1.954	1.928	1.603
μ/mm^{-1}	2.572	2.166	2.371	2.265	1.811
Θ/°	3.968–55.91	2.982–55.892	2.99–55.906	3.946–55.91	3.046–55.7
F(000)	854	5140	5136	5112	2680
Data/restraints/parameters	7328/6/406	10 663/54/726	10 611/96/752	10 680/42/688	13 356/115/792
GOF (F^2)	1.032	0.975	0.893	1.032	0.947
R_1, wR_2 ($I \geq 2\sigma(I)$)	0.0577, 0.1433	0.0470, 0.1159	0.0524, 0.1029	0.0690, 0.1679	0.0678, 0.1582
R_1, wR_2 (all data)	0.0879, 0.1663	0.0718, 0.1263	0.0996, 0.1163	0.1132, 0.1933	0.1152, 0.1783

there is no report of any complex in which the phosphonate group and the bipyridine pocket coordinate at the same time. So far the ligand has solely been used for the preparation of diamagnetic Ru(II) and Zr(IV) complexes, which, however, have not been characterized by single crystal diffraction.[36–38]

Herein we report the synthesis and full characterisation of seven novel compounds incorporating 3d transition metal ions and 4f elements. We were able to prepare 0D and 2D homometallic structures as well as heterometallic 2D and 3D structures with Co, Ni, Gd, Tb and Dy. We obtained single crystal diffraction data for all compounds (Table 1) and investigated the magnetic properties of all the more-dimensional complexes.

Results and discussion

Synthesis

One of the most common and applied methods in phosphonate chemistry is hydrothermal synthesis.[30,39] Unfortunately, these reaction conditions involve the loss of selectivity towards the 4f metals. We decided therefore to employ a different strategy and induced a growth of crystals by either changing the polarity of the solvent or else evaporation of the solvent at elevated temperatures to form the thermodynamically more stable compound. The outcome of the reaction mixture depends on three factors: the ligand/metal ratio, the pH-value and the order of the added metal salts. By varying them, we could observe different connectivity and had hence influence onto the dimensionality up to a certain degree.

Crystal structures

Compound **1a** and **1b** ($[M(\mathbf{H_2L})(H_2O)_4]\cdot 2.5H_2O$; M = Co^{2+} (**a**), Ni^{2+} (**b**)) are isostructural and comprise one metal centre, one twofold deprotonated ligand $(\mathbf{H_2L})^{2-}$ and 6.5 water molecules. The detailed crystal structure can be found in the ESI.† In both cases, the central ion shows an octahedral coordination geometry in which four of the water molecules are included. As expected, the ligand coordinates in an η_2-coordination mode. Despite the large number of possible coordination sites, the complexes are of molecular structure. This emphasizes our earlier statement, that transition metal–phosphonate bonds are rather formed during hydrothermal synthesis, at least under moderate pH conditions. The nitrogen–metal bond lengths of 2.123 Å and 2.139 Å for **1a** and the oxygen–phosphonate bond lengths within the phosphonates indicate an oxidation state of +2 for the metal ions.[40] The positive charge is compensated by the single deprotonated phosphonate groups. Individual complexes are connected *via* hydrogen bonds mediated by water molecules (see Fig. S3 in ESI†).

Compound **2** ($[Gd_2(\mathbf{H_2H'L})_2(\mathbf{H_2H'_2L})(H_2O)_6]Cl_4]\cdot 14H_2O$) forms a two dimensional network. The structure was solved in the space group $P\bar{1}$. The asymmetric unit contains 1.5 ligand molecules with different grades of protonation, one eightfold coordinated gadolinium(III)-ion, ten water molecules from which three are coordinating and two chloride counter ions. A comparison of the oxygen–phosphorus bond lengths reveals that they are either around 1.50 Å or else 1.55 Å. The latter one is the typical bond length for a protonated oxygen atom. Therefore, all phosphonate groups are assumed to be only single deprotonated. Additionally, the nitrogen atoms of the split ligand ($\mathbf{H_2H'_2L}$) are protonated, whereas $(\mathbf{H_2H'L})^-$ shows only one protonated nitrogen, leaving it with a negative charge. Both types of ligands differ as well in their coordination mode. The phosphonate of $\mathbf{H_2H_2'L}$ and the phosphonate of $(\mathbf{H_2H'L})^-$ which is closer to the protonated nitrogen atom are each bridging two lanthanides with two oxygen in a μ_2-mode.

The remaining phosphonate coordinates to one gadolinium ion *via* one oxygen atom, which gives in total five metal–phos-

Open Access Article. Published on 19 July 2016. Downloaded on 12/4/2025 9:06:27 PM.
This article is licensed under a Creative Commons Attribution-NonCommercial 3.0 Unported Licence.

phonate connections. The remaining three coordination sites of the square antiprismatic sphere are occupied by water molecules. Due to the μ_2-briding mode of the individual phosphonate groups, the central ions show a one dimensional I^1 chainlike structure along the *a*-axis, as shown in Fig. 1(c), with a mean distance between two lanthanide ions of 5.212 Å. In Fig. 1(b), the O^1 connection by the bipyridine acting as a tether along the *c*-axis is depicted. The spacing between the chains is on average 11.504 Å. The layers are connected *via* hydrogen bonds forming between the counter ions along the *b*-direction.

Compounds **3a**, **3b** and **3c** ($[MCo(III)(\mathbf{H_2L})_3(H_2O)_2]\cdot 6.5H_2O$; M = Gd^{3+} (**a**), Dy^{3+} (**b**) and Tb^{3+} (**c**), Fig. 2(a)) are two-dimensional heterometallic coordination polymers. The structures were solved in the space group *C*2/*c*. All three complexes are isostructural and differ only in their 4f element. The lanthanides are coordinated in a for lanthanides rather rare seven-fold coordinated capped trigonal prismatic geometry.[41] As expected, the coordination sphere is formed by seven oxygen atoms belonging to different groups. Five of the oxygen atoms belong to five separate phosphonate groups, the remaining two origin from water molecules, leaving one non-coordinating phosphonate group. Similar to compound **2**, all phosphonates are single protonated as indicated by the P–O bond lengths. One trigonal plane and the cap of the coordination polyhedral is built from four phosphonate oxygen atoms, while the other plane includes both water molecules and one ligand molecule. A comparison of the oxygen–lanthanide bond lengths shows, that the average distance to the water molecules are quiet shorter than the bonds to the ligand (2.291 Å and 2.451 Å, respectively). The second metal is chelated in an η_2-coordination mode comparable to compound **1a** and **1b**, but by three bipyridine coordination sites. They form $(Co(\mathbf{H_2L})_3)^{3-}$ building units which connect the incorporated lanthanide ions. The N–Co bond lengths differ significantly from the lengths in the previously described complexes. They range from 1.916(8) Å to 1.950(9) Å with a mean value of 1.933 Å. The origin is found in the oxidation state of the cobalt ion, which oxidizes during the reaction from Co(II) to Co(III). The small differences in bond lengths and the *cis*-angles being close to 90° indicate a good approximation to an ideal octahedral coordination sphere. Fig. 2(b) represents a side view along the *b*-axis of the two-dimensional layers. It is clearly visible, that only five out of six phosphonate groups are coordinating. The remaining group protrudes above and beneath the layer, connecting it by hydrogen bonds between the phosphonate and crystal water to neighbouring arrays. A closer examination of the arrangement within the layer in Fig. 2(c) shows, that the cobalt octahedron form some sort of one-dimensional chain along the *b*-axis. The distance between two terbium polyhedron is 5.514 Å, which is comparably close to the chain in compound **2**. However, they are connected by hydrogen bonds between the phosphonates and show therefore no direct coordinative or covalent contact.

Additionally, the arrangement of the metal centres should rather be described as dimers then chains due to their discontinuous nature: the spacing to the next terbium in the opposite direction is with 11.885 Å much longer.

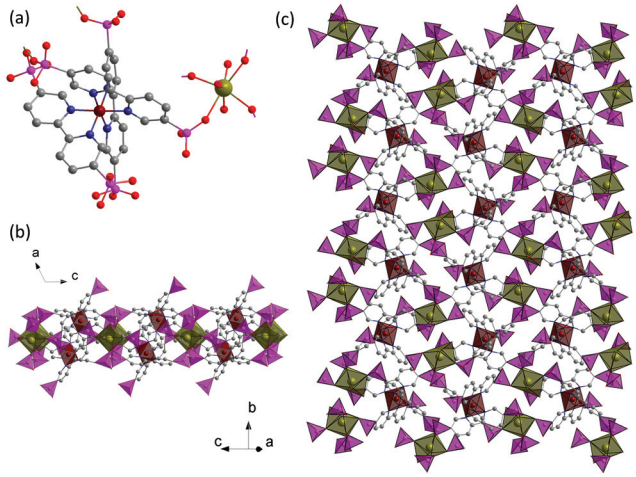

Fig. 2 (a) Asymmetric unit of compound **3c** with broken off bonds. (b) Side view of a layer illustrating the non-coordinating phosphonate groups. (c) Top view of the crystal structure showing the cobalt and terbium chains. Colour code: brown – gadolinium, dark red – cobalt, pink – phosphorus, red – oxygen, dark blue – nitrogen, grey – carbon. Hydrogen atoms and solvent molecules have been omitted for clarity.

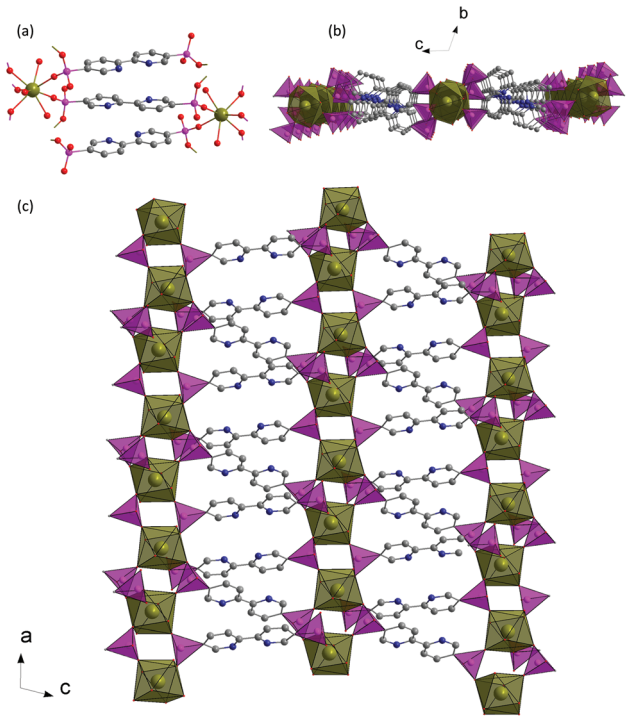

Fig. 1 (a) Primitive cell of compound **2** with broken off bonds. (b) Top view shows the O^1 tethering of the bipyridine backbone. (c) Graphical representation of the I^1 gadolinium chains. Colour code: brown – gadolinium, pink – phosphorus, red – oxygen, dark blue – nitrogen, grey – carbon. Hydrogen atoms and solvent molecules have been omitted for clarity.

 This journal is © The Royal Society of Chemistry 2016

Open Access Article. Published on 19 July 2016. Downloaded on 12/4/2025 9:06:27 PM.
This article is licensed under a Creative Commons Attribution-NonCommercial 3.0 Unported Licence.

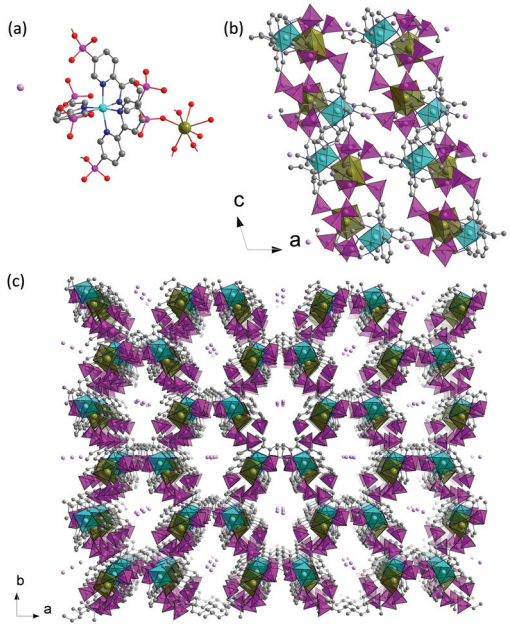

Fig. 3 (a) Cation of the asymmetric unit of compound **4** with broken off bonds. (b) View along the *b*-axis showing the connection of the crooked layers by the $Ni(H_2L)_3$ units. (c) The view along the *c*-axis reveals the three-dimensional structure of the compound and the oval motive it is forming. Colour code: brown polyhedron – gadolinium, light blue polyhedron – nickel, pink polyhedron – phosphorus, rose – sodium, red – oxygen, dark blue – nitrogen, grey – carbon. Hydrogen atoms and solvent molecules have been omitted for clarity.

The asymmetric unit of compound **4** (Fig. 3(a)) has the sum formula $[GdNi(II)(\mathbf{H_2L})_3(H_2O)_3]NaCl{\cdot}6H_2O$. The crystal structure can be solved in the space group *C*2 and forms a three-dimensional coordination polymer by the μ_2-bridging of the gadolinium centres *via* the ligands. The lanthanide ion has, similar to compounds **3a**, **3b** and **3c**, a coordination number of seven and is in a capped trigonal prismatic coordination environment. But in contrast to the three cobalt complexes, the nickel compound shows three lanthanide–water contacts and only four lanthanide–phosphonate connections, leaving two non-coordinating phosphonate groups.

The different connectivity of the phosphonates arises from the different initial pH value due to the use of the chloride metal salt instead of the acetate metal salt and the larger amount of hydrochloric acid which was employed to dissolve the precipitate. As a consequence, the number of phosphonate–metal contacts is reduced. Both trigonal planes of the capped trigonal prism equally consist of two phosphonate groups and one water molecule. The cap is built from a water molecule as well. Again, the nickel ions are coordinated octahedral by the bipyridine coordination sites of the ligand and form building blocks, which connect the gadolinium ions. Due to the different coordination mode of the phosphonates, the motive of a paired chain as in **3a–3c** is not present in this compound. Instead, the two different metal ions Ni^{2+} and Gd^{3+} occur alternating. In Fig. 3(c), a view along the *c*-axis of the crystal structure is shown. It is a representative picture of the three-dimensional structure of this compound and shows the oval pores the structure is forming in this direction. The representation reveals, that the sodium ions are occupying the space within the pores.

Magnetic properties

Magnetic measurements at variable temperatures have been carried out for all more-dimensional compounds. All measurements regarding $\chi_M T$ where conducted under an applied field of 1 kOe in a temperature range between 2 K and 300 K. For compound **2**, a $\chi_M T$ value of 7.76 cm^3 K mol^{-1} was observed at room temperature (Fig. 4), which is in good agreement with the expected values for two uncoupled Gd^{3+} ions (7.88 cm^3 K mol^{-1}, $^8S_{7/2}$, $S = 7/2$, $L = 0$, $g = 2$). Upon decreasing the temperature, the value remains almost constant until 10 K, where it increases abruptly. The increase of the magnetic moment can be attributed to several causes. First, it can be the result of a weak ferromagnetic exchange coupling, occurring between neighbouring gadolinium ions, mediated by the phosphonate groups. In order to quantify these findings, the temperature dependent magnetic molar susceptibility was fitted with the program PHI using an isotropic exchange interaction Hamiltonian $\hat{H}_{EX} = -2J\hat{S}_1{\cdot}\hat{S}_2$.[42]

For the simulation, the structure was considered as a dimer. The largest congruence of the data was obtained with the parameters $J = 0.0076$ cm^{-1} and $g = 1.992$, where the positive sign of the coupling constant indicates that the coupling is indeed of weak ferromagnetic nature. It should be noted, that such small values are more of a qualitative nature. Another reason for the increasing susceptibility at low temperatures could be dipolar coupling. Such magnetic dipole–dipole interaction can occur, when two spin carriers are in very close proximity to each other, which is the case for the gadolinium ions along the I^1 chains in this structure.[43] And finally,

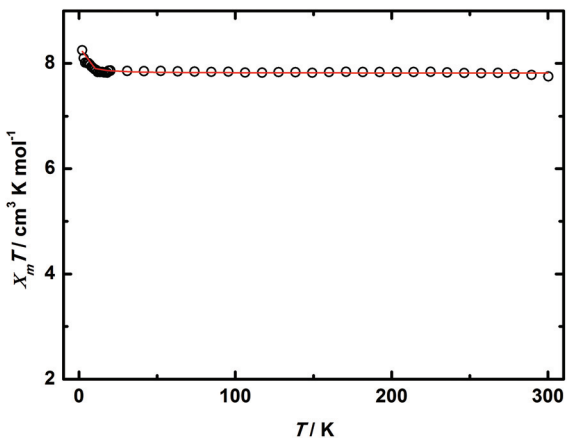

Fig. 4 Temperature dependent measurement of the molar magnetic susceptibility per gadolinium ion for compound **2** in a temperature range between 2 K and 300 K with an applied field of 1 kOe. Black circles represent the experimental data, the red line the simulation with the parameter $g = 1.992$ and $J = 0.0076$ cm^{-1}.

Open Access Article. Published on 19 July 2016. Downloaded on 12/4/2025 9:06:27 PM.
This article is licensed under a Creative Commons Attribution-NonCommercial 3.0 Unported Licence.

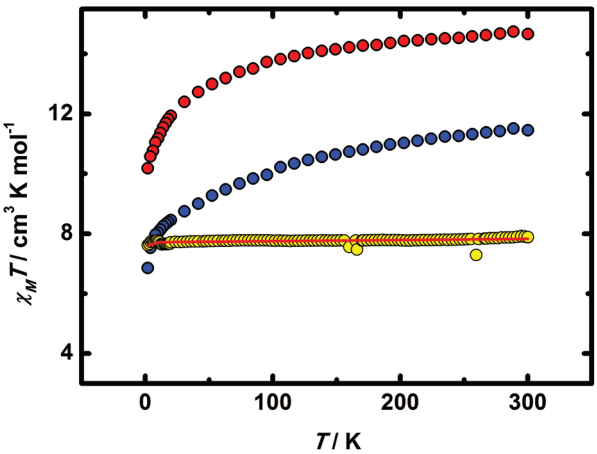

Fig. 5 Temperature dependent measurement of the molar magnetic susceptibility for compounds **3a** (yellow circles), **3b** (red circles) and **3c** (blue circles). The red line represents the fitted of **3a**.

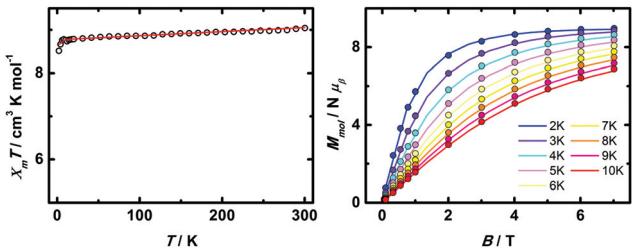

Fig. 6 Representation of the magnetic properties of compound **4**. Left: Variable temperature measurement of the molar susceptibility χ_M. Plot shows the product $\chi_M T$ *vs.* T. Circles represent the experimental data, the line the fit obtained by PHI. Right: Magnetization at different temperatures in an applied external magnetic field between 1 kOe and 70 kOe.

such an increase of $\chi_M T$ could arise from a phase transition the compound undergoes at low temperatures.[44,45]

Fig. 5 shows the magnetic characterization for compounds **3a**, **3b** and **3c** *via* measurements of the magnetic molar susceptibility. The $\chi_M T$ value at room temperature for the isotropic gadolinium complex is with 7.90 cm^3 K mol^{-1} close to the expected value for an uncoupled gadolinium ion (7.88 cm^3 K mol^{-1}, $^8S_{7/2}$, $S = 7/2$, $L = 0$, $g = 2$). The susceptibility remains almost constant during the decline of the temperature until 13 K, where it decreases due to small zero field splitting or saturation effects. For quantification, the magnetic data were fitted using the programme PHI.[42] The obtained parameters are $g = 1.980$ and a temperature independent paramagnetism (TIP) of 3.75×10^{-4}. Fig. 5 shows the magnetic susceptibility for **3b** and **3c** as well. At room temperature, the values of $\chi_M T$ are 14.66 cm^3 K mol^{-1} and 11.45 cm^3 K mol^{-1}, respectively. This is in good agreement with the expected values of 14.17 cm^3 K mol^{-1} for **3b** and 11.82 cm^3 K mol^{-1} for **3c** for uncoupled lanthanides: Tb^{3+} ($^7F_6$, $S = 6$, $L = 3$, $g = 3/2$) and Dy^{3+} ($^6H_{15/2}$, $S = 5/2$, $L = 5$, $g = 4/3$). Upon cooling, a decrease of the $\chi_M T$ value is observed, which is attributed to a progressive depopulation of the Stark levels split due to the ligand field.[43,46,47]

For the field dependent magnetization data at different temperatures for compound **3b** and **3c** see the ESI.† The obtained values for the magnetization are quiet lower than the theoretical saturation values one would expect for an isolated Dy^{3+} ion ($10N\beta$) and Tb^{3+} ion ($9N\beta$). The reason is found again in the magnetic anisotropy with a lower effective spin, and the splitting of the Stark level by the ligand field.[14,48,49]

Compound **4** ([GdNi(II)(**H$_2$L**)$_3$(H$_2$O)$_3$]NaCl·6H$_2$O) shows at room temperature a $\chi_M T$ value of 9.04 cm^3 K mol^{-1} (see Fig. 6), which is in good agreement with the expected values for an uncoupled Gd^{3+}-ion (7.88 cm^3 K mol^{-1}, $^8S_{7/2}$, $L = 0$, $S = 7/2$, $g = 2$) and an uncoupled Ni^{2+}-ion (1.00 cm^3 K mol^{-1}, $^3A_{2g}$, $L = 0$, $S = 1$, $g = 2$). Upon cooling, the value remains almost constant and decreases only slightly to 8.76 cm^3 K mol^{-1} at 6 K, where it declines to a final value of 8.51 cm^3 K mol^{-1} at 2 K, most probably due to zero field splitting. The field dependent magnetization was measured in a temperature range from 2 K up to 10 K. At low fields, M rapidly increases until a maximum of $8.97N\beta$ and $6.78N\beta$ is slowly reached at 70 kOe (2 K and 10 K, respectively). Again, the values are in good agreement with the expected values at 2 K and 10 K for an uncoupled Gd^{3+} ion ($6.98N\beta$ and $5.73N\beta$) and an uncoupled Ni^{2+} ion ($1.98N\beta$ and $1.10N\beta$). The data were fitted using the program PHI. The best accordance of the data was obtained with the fitting parameters $g(Gd^{3+}) = 1.980$, $g(Ni^{2+}) = 2.0438$ and a TIP of 9.469×10^{-4}. Due to the similarity of the coordinative environment between compound **3a** and **4**, the $g(Gd^{3+})$ value from **3a** was used. The magnetic data of compound **4** and compounds **3a**, **3b** and **3c** confirm the oxidation states of the nickel and cobalt ions being +II and +III, respectively. In a strongly split ligand field, Co(III) is found almost exclusively in the diamagnetic low-spin state due to the large ligand field stabilisation energy arising from the electronic configuration $t_{2g}^6\ e_g^0$.

The $\chi_M T$ value of compound **3a** reflects the absence of another spin carrier additional to the gadolinium ion. The oxidation during the reaction is promoted by two circumstances: first, by the elevated temperature during the crystallization. And second, due to the electronic configuration of $t_{2g}^6\ e_g^1$ in an octahedral coordination environment caused by a strong ligand field, such as from the 2,2′-bipyridine, the Co(II) ion seeks for a Jahn–Teller distortion to remove the degeneracy of the e_g-orbitals.[50,51] This is hindered by the rigid ligand backbone, which disallows the elongation along a Jahn–Teller axis. The electronic configuration of an octahedral coordinated Ni(II) ion ($t_{2g}^6\ e_g^2$) is much more preferential compared to a Ni(III) ion ($t_{2g}^6\ e_g^1$), which would be forced by the Jahn–Teller effect into a for the system not realizable distorted octahedral coordination geometry.

Conclusions

In conclusion, we were able to identify and employ a highly versatile ligand system for the synthesis of several more-dimen-

Open Access Article. Published on 19 July 2016. Downloaded on 12/4/2025 9:06:27 PM.
This article is licensed under a Creative Commons Attribution-NonCommercial 3.0 Unported Licence.

sional 3d and 4f metal complexes. By taking advantage of the different coordination properties, which are offered by the functionalities of the ligand, we prepared several compounds of homometallic and heterometallic nature. In compound **2**, the metal ions are connected by phosphonate groups and form one-dimensional chains. They are tethered *via* the ligands backbone, which space them by a distance of 11.504 Å. The lanthanides in the heterometallic compounds **3a**, **3b**, **3c** and **4** are in a capped trigonal prismatic coordination geometry and show a rare coordination number of seven. Magnetic measurements were carried out for all the more-dimensional complexes. Compound **2** revealed an increase of the magnetic molar susceptibility at low temperatures, which can be attributed to weak ferromagnetic exchange interactions. Compounds **3a**, **3b**, **3c** and **4** showed that, depending on the metal, an *in situ* oxidation during the synthesis was observed due to the possible occurrence of a Jahn–Teller effect. Studies of the magnetization at various temperatures of compounds **3b** and **3c**, which contain anisotropic lanthanides, showed a split of the Stark level at low temperatures caused by the ligand field. Further syntheses involving the use of various metal/metal/ligand ratios and different reaction conditions are underway in our laboratory to widen the diversity of complexes which can be prepared by employing the ligand system and improve on the magnetic properties.

Experimental

General methods and materials

All chemicals were purchased from Alfa Aesar, Deutero, Fisher Chemicals, Sigma–Aldrich and Acros Organics and used without further purification. The NMR spectra were recorded at room temperature by using a Bruker DRX 400 spectrometer and analysed with the program MestReNova.[52] Magnetic susceptibility data was collected with a Quantum Design SQUID magnetometer MPMSXL in a temperature range of 2–300 K with an applied field of 10 kOe. Elemental analyses (C, H, N and S) were measured at the micro analytical laboratories of the Johannes Gutenberg University Mainz. X-ray diffraction data were collected at 173 K with a Bruker SMART diffractometer and a STOE IPDS 2 T at the Johannes Gutenberg University Mainz. The structures were solved with ShelXT and refined with ShelXL 2013 with the program Olex2. CCDC 1477300 (for **1a**), 1477301 (for **1b**), 1477302 (for **2**), 1477303 (for **3a**), 1477304 (for **3b**), 1477305 (for **3c**), 1477306 (for **3a**) and 1477307 (for **SI1**) contain the supplementary crystallographic data for this paper.

Ligand synthesis. The ligand was prepared as reported in the literature:[35] with a selective 5,5′-dibromination of 2,2′-bipyridine hydrobromide,[53] followed by a palladium catalysed phosphonation, the respective phosphonic dialkyl ester 5,5′-bis(diethylphosphonato)-2,2′-bipyridine was obtained as precursor. The desired ligand $\mathbf{H_4L}$ (2,2′-bipyridinyl-5,5′-diphosphonic acid) was accessible by hydrolyzation using TMS-Br according to the literature.[54] It was isolated as $\mathbf{H_3H'L}$ with **H** being a phosphonic acid proton and **H′** being a nitrogen bound proton as depicted in Scheme 1. The crystal structure of $\mathbf{H_3H'L}$ can be found in the ESI (Fig. S1†).

Complex synthesis. For the preparation of compound **1a**, 0.2 mmol $\mathbf{H_3H'L}$ (63.23 mg) were added to a mixture of 3 mL H_2O and 40 μL of concentrated aqueous ammonia. After filtration, a solution of 0.2 mmol $Co(Ac)_2{\cdot}4H_2O$ (49.82 mg) in 3 mL H_2O was added dropwise and under stirring. An immediate change of colour from pale pink to an intense orange was visible. The viol was left to stand for the solvent to evaporate slowly. Single crystals of orange colour suitable for single crystal XRD (see ESI Fig. S2†) grew after several days. Yield: 41.57 mg, 46.7%, $C_{10}H_{11}N_2O_{7.5}P_2Co$ ($[Co(H_2L)]{\cdot}1.5H_2O$) (400.08): calcd C 30.02, H 2.77, N 7.00; found C 30.30, H 3.02, N 6.96.

Compound **1b** (Fig. S4†) was prepared according to the procedure of **1a** by using 0.2 mmol $NiCl_2{\cdot}6H_2O$ (47.59 mg). Upon addition of ligand and metal, a colour change from pale green to light blue was observed. Yield: 37.72 mg, 42.39%, $C_{10}H_{15}N_2O_{9.5}P_2Ni$ ($[Ni(\mathbf{H_2L})]{\cdot}3.5H_2O$) (435.87): calcd C 27.56, H 3.47, N 6.43; found C 27.74, H 3.43, N 6.47.

Compound **2** was prepared by adding solution of 0.1 mmol $Gd(NO_3)_3{\cdot}5H_2O$ (43.33 mg) in 3 mL H_2O to a mixture of 0.15 mmol $\mathbf{H_3H'L}$ (47.42 mg) in 3 mL H_2O. Immediately, a white solid precipitated. The precipitate was separated from the solution by centrifugation. After the emulsification in 4 mL water, concentrated HCl (0.5 mL) was added to dissolve the solid, giving a clear solution. Acetonitrile (2 mL) was added and the viol was left to stand for six days, giving colourless crystals suitable for single crystal XRD. Yield: 81.51 mg, 58.13% $C_{30}H_{38.5}N_6P_6O_{23.25}Gd_2Cl_4$ ($[Gd_2(\mathbf{H_2H'L})_2(\mathbf{H_2H'_2L})]Cl_4]{\cdot}5.25H_2O$) (1497.31): calcd C 24.07, H 2.59, N 5.61; found C 23.81, H 2.74, N 5.91.

Compound **3a**, **3b** and **3c** were prepared by using the following procedure: 0.3 mmol $\mathbf{H_3H'L}$ (94.84 mg) were dissolved in 3 mL H_2O and 40 μL of concentrated ammonia were added. After filtration, 0.1 mmol $Co(Ac)_2{\cdot}4H_2O$ (24.91 mg) dissolved in 4 mL H_2O were added, whereupon the solution turned orange. The addition of 0.1 mmol $M(NO_3)_3{\cdot}xH_2O$ (**3a**: M = Gd, X = 5, m = 43.33 mg; **3b**: M = D, X = 1, m = 36.65 mg; **3c**: M = Tb, X = 1, m = 36.30 mg) dissolved in 4 mL H_2O resulted in an immediate precipitation of a white solid, which was dissolved by the addition of 0.5 mL concentrated HCl. The viol was placed in an oven set to 80 °C for 18 h, after which isostructural single crystals suitable for single crystal XRD of orange colour with similar morphology were obtained. **3a**: Yield: 50.17 mg, 43.3%. $C_{30}H_{40}N_6P_6O_{26}CoGd$ ($[GdCo(\mathbf{H_2L})_3]{\cdot}8H_2O$) (1302.69): calcd C 27.66, H 3.09, N 6.45; found C 27.64, H 3.20, N 6.45. **3b**: Yield: 54.41 mg, 46.8%, $C_{30}H_{34}N_6P_6O_{23}CoDy$ ($[DyCo(\mathbf{H_2L})_3]{\cdot}5H_2O$) (1253.89): calcd C 28.74, H 2.73, N 6.70; found C 28.60, H 2.65, N 6.74. **3c**: Yield: 44.35 mg, 38.2%, $C_{30}H_{38}N_6P_6O_{25}CoTb$ ($[DyCo(H_2L)_3]{\cdot}7H_2O$) (1286.35): calcd C 28.01, H 2.98, N 6.53; found C 28.06, H 2.93, N 6.59.

For the preparation of compound **4**, 0.15 mmol $\mathbf{H_3H'L}$ (47.42 mg) were dissolved in 2 mL H_2O and 0.32 mmol of sodium hydroxide were added. After filtration, 0.05 mmol

Open Access Article. Published on 19 July 2016. Downloaded on 12/4/2025 9:06:27 PM.
This article is licensed under a Creative Commons Attribution-NonCommercial 3.0 Unported Licence.

$NiCl_2 \cdot 6H_2O$ (11.90 mg) dissolved in 2 mL H_2O were added. The addition of 0.05 mmol $Gd(NO_3)_3 \cdot 5H_2O$ dissolved in 2 mL H_2O resulted in an immediate precipitation of a white solid, which was dissolved by the addition of 0.4 mL concentrated HCl. The viol was placed in an oven set to 80 °C, where the solvent evaporated and the solution concentrated until a remaining volume of approximately 1.5 mL and then left to stand at room temperature. Single crystals of pale orange suitable for single crystal XRD could be obtained after one day. Yield: 26.58 mg, 43.7%. $C_{30}H_{35}N_6P_6O_{23}NiGdNaCl$ ($[GdNi(\mathbf{H_2L})_3] \cdot 5H_2O$) (1307.85): calcd C 27.55, H 2.70, N 6.43; found C 27.39, H 2.88, N 6.51.

Acknowledgements

Dr Dieter Schollmeyer and Regine Jung-Pothmann are kindly acknowledged for the support with the crystallographic data.

Notes and references

1 J. C. Tan and A. K. Cheetham, *Chem. Soc. Rev.*, 2011, **40**, 1059–1080.
2 L. D. Carlos, R. A. Ferreira, V. De Zea Bermudez, B. Julian-Lopez and P. Escribano, *Chem. Soc. Rev.*, 2011, **40**, 536–549.
3 M. T. Wharmby, J. P. S. Mowat, S. P. Thompson and P. A. Wright, *J. Am. Chem. Soc.*, 2011, **133**, 1266–1269.
4 A. Kondo, T. Satomi, K. Azuma, R. Takeda and K. Maeda, *Dalton Trans.*, 2015, **44**, 12717–12725.
5 S. Jones, J. M. Vargas, S. Pellizzeri, C. J. O'Connor and J. Zubieta, *Inorg. Chim. Acta*, 2013, **395**, 44–57.
6 M. Pramanik, M. Nandi, H. Uyama and A. Bhaumik, *Catal. Sci. Technol.*, 2012, **2**, 613–620.
7 H. Tan, W. Chen, D. Liu, X. Feng, Y. Li, A. Yan and E. Wang, *Dalton Trans.*, 2011, **40**, 8414–8418.
8 L. D. Carlos, R. A. S. Ferreira, V. D. Bermudez, B. Julian-Lopez and P. Escribano, *Chem. Soc. Rev.*, 2011, **40**, 536–549.
9 K. J. Gagnon, H. P. Perry and A. Clearfield, *Chem. Rev.*, 2012, **112**, 1034–1054.
10 K. Maeda, *Microporous Mesoporous Mater.*, 2004, **73**, 47–55.
11 K. Maeda, Y. Kiyozumi and F. Mizukami, *J. Phys. Chem. B*, 1997, **101**, 4402–4412.
12 Y.-S. Ma, H. Li, J.-J. Wang, S.-S. Bao, R. Cao, Y.-Z. Li, J. Ma and L.-M. Zheng, *Chem. – Eur. J.*, 2007, **13**, 4759–4769.
13 L. Rosado Piquer and E. C. Sañudo, *Dalton Trans.*, 2015, **44**, 8771–8780.
14 J. Tang, I. Hewitt, N. T. Madhu, G. Chastanet, W. Wernsdorfer, C. E. Anson, C. Benelli, R. Sessoli and A. K. Powell, *Angew. Chem., Int. Ed.*, 2006, **45**, 1729–1733.
15 G. Novitchi, G. Pilet, L. Ungur, V. V. Moshchalkov, W. Wernsdorfer, L. F. Chibotaru, D. Luneau and A. K. Powell, *Chem. Sci.*, 2012, **3**, 1169–1176.
16 J. A. Sheikh, A. Adhikary, H. S. Jena, S. Biswas and S. Konar, *Inorg. Chem.*, 2014, **53**, 1606–1613.
17 Y. Z. Zheng, M. Evangelisti and R. E. P. Winpenny, *Angew. Chem., Int. Ed.*, 2011, **50**, 3692–3695.
18 S. Hu, L. Yun, Y. Z. Zheng, Y. H. Lan, A. K. Powell and M. L. Tong, *Dalton Trans.*, 2009, 1897–1900.
19 M. Andruh, J.-P. Costes, C. Diaz and S. Gao, *Inorg. Chem.*, 2009, **48**, 3342–3359.
20 J. A. Sheikh, S. Goswami and S. Konar, *Dalton Trans.*, 2014, **43**, 14577–14585.
21 Y. Bing, N. Xu, W. Shi, K. Liu and P. Cheng, *Chem. – Asian J.*, 2013, **8**, 1412–1418.
22 M. Kurmoo, *Chem. Soc. Rev.*, 2009, **38**, 1353–1379.
23 L. J. Murray, M. Dinca and J. R. Long, *Chem. Soc. Rev.*, 2009, **38**, 1294–1314.
24 A. Bencini, C. Benelli, A. Caneschi, R. L. Carlin, A. Dei and D. Gatteschi, *J. Am. Chem. Soc.*, 1985, **107**, 8128–8136.
25 Z.-G. Gu and S. C. Sevov, *J. Mater. Chem.*, 2009, **19**, 8442–8447.
26 B. Zhao, P. Cheng, Y. Dai, C. Cheng, D. Z. Liao, S. P. Yan, Z. H. Jiang and G. L. Wang, *Angew. Chem., Int. Ed.*, 2003, **42**, 934–936.
27 T. K. Prasad, M. V. Rajasekharan and J. P. Costes, *Angew. Chem., Int. Ed.*, 2007, **46**, 2851–2854.
28 A. C. Rizzi, R. Calvo, R. Baggio, M. T. Garland, O. Peña and M. Perec, *Inorg. Chem.*, 2002, **41**, 5609–5614.
29 R. A. Palmer and T. S. Piper, *Inorg. Chem.*, 1966, **5**, 864–878.
30 V. Lopez-Diaz, T. M. Smith Pellizerri, M. D. Lijewski, K. Ruhlandt and J. Zubieta, *Inorg. Chim. Acta*, 2016, **441**, 109–116.
31 E. M. Pineda, F. Tuna, Y.-Z. Zheng, S. J. Teat, R. E. P. Winpenny, J. Schnack and E. J. L. McInnes, *Inorg. Chem.*, 2014, **53**, 3032–3038.
32 M. Bartholomä, H. Chueng, S. Pellizzeri, K. Ellis-Guardiola, S. Jones and J. Zubieta, *Inorg. Chim. Acta*, 2012, **389**, 90–98.
33 E. Fernández-Zapico, J. Montejo-Bernardo, A. Fernández-González, J. R. García and S. García-Granda, *J. Solid State Chem.*, 2015, **225**, 285–296.
34 G. Guerrero, J. G. Alauzun, M. Granier, D. Laurencin and P. H. Mutin, *Dalton Trans.*, 2013, **42**, 12569–12585.
35 V. Penicaud, F. Odobel and B. Bujoli, *Tetrahedron Lett.*, 1998, **39**, 3689–3692.
36 F. Odobel, B. Bujoli and D. Massiot, *Chem. Mater.*, 2001, **13**, 163–173.
37 I. Gillaizeau-Gauthier, F. Odobel, M. Alebbi, R. Argazzi, E. Costa, C. A. Bignozzi, P. Qu and G. J. Meyer, *Inorg. Chem.*, 2001, **40**, 6073–6079.
38 H. Zabri, I. Gillaizeau, C. A. Bignozzi, S. Caramori, M.-F. Charlot, J. Cano-Boquera and F. Odobel, *Inorg. Chem.*, 2003, **42**, 6655–6666.
39 S. Khanra, S. Konar, A. Clearfield, M. Helliwell, E. J. L. McInnes, E. Tolis, F. Tuna and R. E. P. Winpenny, *Inorg. Chem.*, 2009, **48**, 5338–5349.
40 A. Rajput and R. Mukherjee, *Coord. Chem. Rev.*, 2013, **257**, 350–368.
41 *Comprehensive coordination chemistry II: from biology to nanotechnology*, ed. J. A. McCleverty and T. J. Meyer, Elsevier Pergamon, Amsterdam, Boston, 2004.

 This journal is © The Royal Society of Chemistry 2016

Open Access Article. Published on 19 July 2016. Downloaded on 12/4/2025 9:06:27 PM.
This article is licensed under a Creative Commons Attribution-NonCommercial 3.0 Unported Licence.

42 N. F. Chilton, R. P. Anderson, L. D. Turner, A. Soncini and K. S. Murray, *J. Comput. Chem.*, 2013, **34**, 1164–1175.
43 W. Haase, *Ber. Bunsen-Ges. Phys. Chem.*, 1994, **98**, 1208–1208.
44 A.-M. Pütz, L. M. Carrella and E. Rentschler, *Dalton Trans.*, 2013, **42**, 16194–16199.
45 C. L. Calvin, *Magnetochemistry*, Springer Verlag, New York, Heidelberg, Tokyo, 1986.
46 Y.-L. Hou, G. Xiong, B. Shen, B. Zhao, Z. Chen and J.-Z. Cui, *Dalton Trans.*, 2013, **42**, 3587–3596.
47 F. Gao, Y.-Y. Li, C.-M. Liu, Y.-Z. Li and J.-L. Zuo, *Dalton Trans.*, 2013, **42**, 11043–11046.
48 F. Yang, Q. Zhou, G. Zeng, G. Li, L. Gao, Z. Shi and S. Feng, *Dalton Trans.*, 2013, **43**, 1238–1245.
49 S. Osa, T. Kido, N. Matsumoto, N. Re, A. Pochaba and J. Mrozinski, *J. Am. Chem. Soc.*, 2004, **126**, 420–421.
50 H. A. Jahn and E. Teller, *Proc. R. Soc. London, Ser. A*, 1937, **161**, 220–235.
51 H. A. Goodwin, in *Spin Crossover in Transition Metal Compounds I*, ed. P. Gütlich and H. A. Goodwin, Springer, Berlin Heidelberg, 2004, pp. 59–90.
52 J. C. Cobas and F. J. Sardina, *Concepts Magn. Reson., Part A*, 2003, **19A**, 80–96.
53 A. B. Zdravkov and N. N. Khimich, *Russ. J. Org. Chem.*, 2006, **42**, 1200–1202.
54 C. E. McKenna, M. T. Higa, N. H. Cheung and M.-C. McKenna, *Tetrahedron Lett.*, 1977, **18**, 155–158.